

Spin nematics, valence-bond solids and spin liquids in $\text{SO}(N)$ quantum spin models on the triangular lattice

Ribhu K. Kaul

Department of Physics & Astronomy, University of Kentucky, Lexington, KY-40506-0055

We introduce a simple model of $\text{SO}(N)$ spins with two-site interactions which is amenable to quantum Monte-Carlo studies without a sign problem on *non-bipartite* lattices. We present numerical results for this model on the two-dimensional triangular lattice where we find evidence for a spin nematic at small N , a valence-bond solid (VBS) at large N and a quantum spin liquid at intermediate N . By the introduction of a sign-free four-site interaction we uncover a rich phase diagram with evidence for both first-order and exotic continuous phase transitions.

The destruction of magnetic order by quantum fluctuations in spin systems is frequently invoked as a route to exotic condensed matter physics such as spin liquid phases and novel quantum critical points [1–3]. The most commonly studied spin Hamiltonians have symmetries of the groups $\text{SO}(3)$ and $\text{SU}(2)$ which describe the rotational symmetry of 3-dimensional space. Motivated both by theoretical and experimental [4] interest, spin models with larger- N symmetries have been introduced, e.g. extensions of $\text{SU}(2)$ to $\text{SU}(N)$ [5–8] or $\text{Sp}(N)$ [9].

The extension of $\text{SO}(3)$ to $\text{SO}(N)$ is an independent large- N enlargement of symmetry, with its own physical motivations [10]. While there have been many studies of $\text{SO}(N)$ spin models in one dimension [11–13], our understanding of their ground states and quantum phase transitions in higher dimension is in its infancy. To this end, we introduce here a simple $\text{SO}(N)$ spin model that surprisingly is sign free on *any* non-bipartite lattice. This model provides us with a new setting in which the destruction of magnetic order can be studied in higher dimensions using *unbiased* methods. As an example of interest, we present the results of a detailed study of the phase diagram of the our $\text{SO}(N)$ anti-ferromagnet on the two-dimensional triangular lattice.

Models. – Consider a triangular lattice, each site of which has a Hilbert state of N states, we will denote the state of site j as $|\alpha\rangle_j$ ($1 \leq \alpha \leq N$). Define the $N(N-1)/2$ generators of $\text{SO}(N)$ on site i as $\hat{L}_i^{\alpha\beta}$ with $\alpha < \beta$; they will be chosen in the fundamental representation on all sites: $\hat{L}_j^{\alpha\beta}|\gamma\rangle_j = i\delta_{\beta\gamma}|\alpha\rangle_j - i\delta_{\alpha\gamma}|\beta\rangle_j$. Now consider the following $\text{SO}(N)$ [14] symmetric lattice model for $N \geq 3$,

$$\hat{H}_J = -\frac{J}{N^2 - 2N} \sum_{\langle ij \rangle} (\hat{L}_i \cdot \hat{L}_j)^2, \quad (1)$$

where the “.” implies a summation over the $N(N-1)/2$ generators and $\langle ij \rangle$ is the set of nearest neighbors. To see that \hat{H}_J does not suffer from the sign problem, define a “singlet” state on a bond, $|S_{ij}\rangle \equiv \frac{1}{\sqrt{N}} \sum_{\alpha} |\alpha\alpha\rangle_{ij}$ and the singlet projector $\hat{P}_{ij} = |S_{ij}\rangle\langle S_{ij}|$. Using these operators and ignoring a constant shift we find the simple form [15],

$$\hat{H}_J = -J \sum_{\langle ij \rangle} \hat{P}_{ij}. \quad (2)$$

We make four observations: First, it is possible to create an $\text{SO}(N)$ spin singlet with only two spins for all N (in contrast to $\text{SU}(N)$ where N fundamental spins are required to create a singlet); Second Eq. (1) being a sum of projectors on this two-site singlet is the simplest $\text{SO}(N)$ coupling, despite it being a biquadratic interaction in the generators $\hat{L}^{\alpha\beta}$; Third, since the singlet has a positive expansion, \hat{H}_J is Marshall positive on *any* lattice; Fourth, on bipartite lattices \hat{H}_J is equivalent to the familiar $\text{SU}(N)$ anti-ferromagnet [6], i.e. the obvious $\text{SO}(N)$ of Eq. (1) is enlarged to an $\text{SU}(N)$ symmetry. Since the bipartite $\text{SU}(N)$ case has been studied in great detail in past work on various lattices [7, 16–23], we shall concern ourselves here with the non-bipartite $\text{SO}(N)$ case which is relatively unexplored.

Phases of \hat{H}_J : Starting at $N = 3$, Eq. (1) becomes $\hat{H} = -\frac{J}{3} \sum_{\langle ij \rangle} (\vec{S}_i \cdot \vec{S}_j)^2$ with \vec{S} the familiar $S = 1$ representation of angular momentum. Previous numerical work has shown that this triangular lattice $S = 1$ biquadratic model [24, 25] has an $\text{SO}(3)$ symmetry breaking “spin nematic” magnetic ground state (we shall denote this phase by SN). The ground state of \hat{H}_J for $N > 3$ has not been studied in the past.

In the large- N limit, analogous to previous work for $\text{SU}(N)$ anti-ferromagnets on bipartite lattices [26], the ground state is infinitely degenerate and consists of dimer coverings where each dimer is in $|S_{ij}\rangle$. At leading order in $1/N$, \hat{H}_J introduces off-diagonal moves which re-arrange parallel dimers around a plaquette, mapping \hat{H}_J at large- N to a quantum dimer model on the triangular lattice with only a kinetic term,

$$\hat{H}_{\text{QDM}} = -t \sum_{\text{plaq}} \left\{ \left(\langle \overrightarrow{\rangle}_i \langle \overleftarrow{\rangle}_i + \text{h.c.} \right) \right\} \quad (3)$$

where the sum on plaquettes includes all closed loops of length four on the triangular lattice. The ground state of this model has been found in previous analytic [27] and numerical work [28] to be a $\sqrt{12} \times \sqrt{12}$ valence bond solid (VBS), breaking the lattice translation symmetry. We thus expect that at large but finite values of N , \hat{H}_J should restore its $\text{SO}(N)$ symmetry and enter this same VBS state.

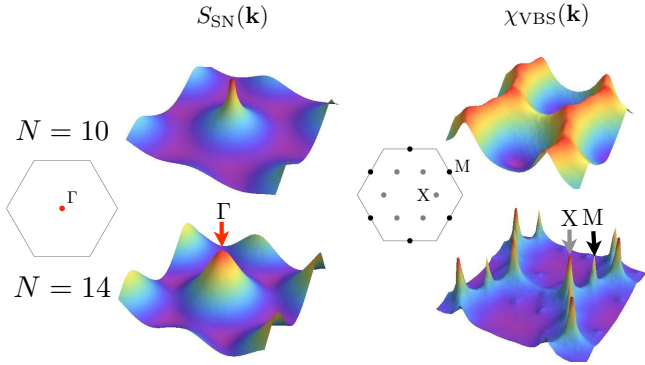


FIG. 1. Equal time structure factors for SN order [$S_{SN}(\mathbf{k})$], and susceptibility for VBS order [$\chi_{VBS}(\mathbf{k})$] shown for $N = 10$ and $N = 14$, for the \hat{H}_J model, Eq. (1) with $L = 48$. The Bragg peaks for SN (VBS) weaken (sharpen) with increasing N . The cartoon of the Brillouin zones shows the location of the ordering vectors of both order parameters. Quantitative finite size scaling of these orders is shown in Fig. 2.

Since \hat{H}_J has SN order for $N = 3$ and is expected to have a non-magnetic VBS at large- N , it is interesting to ask what the nature of the transition at which SN magnetism is destroyed. The answer to this question is unclear based on current theoretical ideas and is best settled by unbiased numerical simulations. Exploiting that \hat{H}_J has no sign problem we study it as a function of N on $L \times L$ lattices at temperature β by unbiased stochastic series expansion [29] quantum Monte Carlo simulations, with a previously described algorithm [24]. The SN state is described by the matrix order parameter $\hat{Q}_{\alpha\beta} = |\alpha\rangle\langle\beta| - \frac{1}{N}$. The static structure factor, $S_{SN}(\mathbf{k}) = \frac{1}{N_{site}^2} \sum_{ij} e^{i\mathbf{k}\cdot(\mathbf{r}_i-\mathbf{r}_j)} \langle \hat{Q}_{\alpha\alpha}(i) \hat{Q}_{\alpha\alpha}(j) \rangle$ is used to detect SN order. For the VBS order, we construct the \mathbf{k} dependent susceptibility of dimer-dimer correlation functions in the usual way from imaginary time-displaced operators: $\chi_{VBS}(\mathbf{k}) = \frac{1}{N_{site}^2} \sum_{ij} e^{i\mathbf{k}\cdot(\mathbf{r}_i-\mathbf{r}_j)} \frac{1}{\beta} \int d\tau \langle \hat{P}_{\mathbf{r}_i, \mathbf{r}_i+\hat{x}}(\tau) \hat{P}_{\mathbf{r}_j, \mathbf{r}_j+\hat{x}}(0) \rangle$. Throughout this paper we have fixed $\beta = L$ for our finite size scaling [15].

As shown in Fig. 1, a peak in $S_{SN}(\mathbf{k})$ is found at the Γ point. Comparing the data at $N = 10$ and $N = 14$, already qualitatively it is possible to see the peak in $S_{SN}(\mathbf{k})$ softens as N is increased. In contrast $\chi_{VBS}(\mathbf{k})$ develops sharp peaks at the X and M points as N is increased. These are precisely the momenta at which previous numerical studies of the triangular lattice quantum dimer model Eq. (3) have observed Bragg peaks [28], validating the large- N mapping to Eq. (3) made earlier. To detect at which N , the magnetic order is destroyed and the VBS order first sets in, we study the ratio, $R_{SN} = 1 - \frac{S_{SN}(\Gamma + \mathbf{a}2\pi/L)}{S_{SN}(\Gamma)}$ (where $\mathbf{a} \equiv \mathbf{x} - \mathbf{y}/\sqrt{3}$) as a function of L . R_{SN} must diverge in a phase in which the Bragg peak height scales with volume and becomes

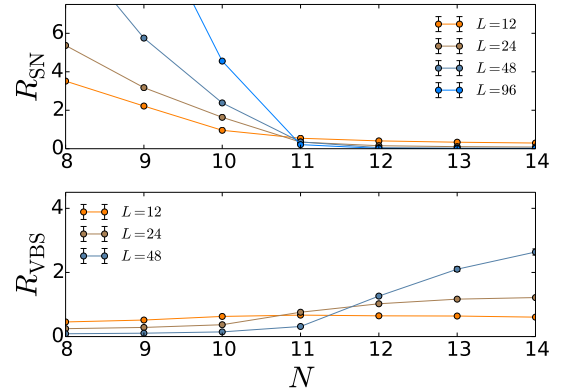


FIG. 2. Crossing plots of the ratios R_{SN} and R_{VBS} as a function of the discrete variable N for the \hat{H}_J model. It is seen that spin nematic order is present for $N \leq 10$. VBS order on the other hand is present for $N \geq 12$. $N = 11$ has no M or VBS order. We present evidence that this phase is a QSL (see text).

infinitely sharp. On the other hand it must go to zero in a phase in which the correlation length is finite and the height and width of the Bragg peak saturate with system size. At a critical point standard finite size scaling arguments imply that the ratio, R_{SN} becomes volume independent. All of these facts together imply a crossing in this quantity for different L . Fig. 2 shows the R_{SN} and R_{VBS} ratios (an analogous quantity constructed for the VBS order from $\chi_{VBS}(\mathbf{k})$ close to the M -point) as a function of the discrete variable N for different L . The data for R_{SN} shows that the magnetic order is present for $N \leq 10$. The R_{VBS} data shows that the long-range VBS order is present for $N \geq 12$. Together the data for both ratios show definitively that $N = 11$ has neither VBS or M order. As we shall substantiate below, at $N = 11$, \hat{H}_J is in a quantum spin-liquid (QSL) phase.

J-Q models: In order to clarify the global phase diagram of $SO(N)$ anti-ferromagnets and access the quantum phase transitions between the SN, VBS and QSL phases found in \hat{H}_J , it is of interest to find an interaction that can tune between these phases at *fixed N*. In order to be meaningful, the new coupling must preserve all the symmetries of \hat{H}_J . To this end, we introduce and study a generalization of the four-site Q term of $SU(2)$ spins [30],

$$\hat{H}_Q = -Q \sum_{\langle i j k l \rangle} \left(\hat{P}_{ij} \hat{P}_{kl} + \hat{P}_{il} \hat{P}_{jk} \right) \quad (4)$$

where the sum includes elementary plaquettes of length four on the triangular lattice (with periodic boundary conditions on an $L \times L$ system there are $3L^2$ such plaquettes). For a fixed- N , \hat{H}_Q provides a tuning parameter which preserve both the internal and lattice symmetries of \hat{H}_J and hence allows us to study the generic phase diagram of $SO(N)$ magnets. A summary of the phase

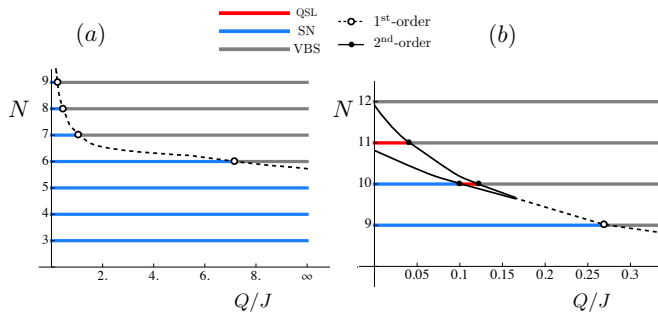


FIG. 3. Phase diagram of \hat{H}_{JQ} [Eqs. (2,4)] for different values of N . The left panel shows the phase diagram for small N , where a first order SN-VBS transition is found for $6 \leq N \leq 9$, (see Fig. 4). As N is increased we find the first order transition weakens. The right panel shows how an intermediate QSL phase emerges for $N = 10$ and $N = 11$. Transitions from the QSL to both SN and VBS phases are continuous on the large systems studied, see Fig. 5.

diagram of \hat{H}_{JQ} in the N - Q/J plane is in Fig. 3: The Q -interaction destroys the SN order and gives way to VBS order only for $N \geq 6$. We have found evidence for direct first-order SN-VBS transitions for $6 \leq N < 10$ and new continuous SN-QSL and SN-VBS transitions for $N = 10$ and $N = 11$.

As an example of our observed first-order behavior we present in Fig. 4, our study of the $N = 7$ QMC data for the spin stiffness $\rho_s \equiv \langle W_x^2 \rangle / L$ (where W_x is the winding number of the spin world lines), which acts as a sensitive order parameter for the SN phase, and the VBS order parameter $O_{\text{VBS}}^2 \equiv \chi_{\text{VBS}}(\mathbf{M})$. Clear evidence for a direct first order SN-VBS transition at $N = 7$ is found.

The nature of the transition changes at $N = 10$, where evidence for two phase transitions is found. As shown in Fig. 5 the SN order vanishes at a Q/J smaller than the value at which VBS order develops. Although the difference is small for $N = 10$, it is significant. The data for $N = 11$ in Fig. 5 shows that the SN and VBS orders do not vanish at the same point. In fact R_{SN} indicates that the SN order has vanished already at $Q/J = 0$, consistent with our previous analysis of \hat{H}_J . As illustrated by the dashed and solid lines in Fig. 3, the appearance of the QSL phase is consistent with a global phase diagram for the $\text{SO}(N)$ magnets.

QSL phase and criticality: We have identified the ground state between SN and VBS as a QSL, since it does not show evidence for any Landau-order. Were the intermediate phase characterized by a conventional order parameter, we would have expected strong first order transitions of the kind between SN and VBS (see Fig. 4), instead we find continuous transitions.

There are field theoretic reasons to expect a QSL on quantum disordering a spin nematic. The long-distance

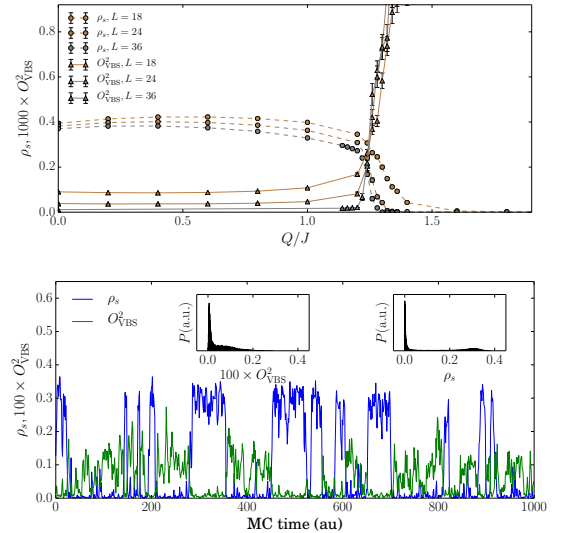


FIG. 4. First-order SN to VBS transition in H_{JQ} at $N = 7$. The upper panel shows the VBS order parameter and the stiffness as a function for Q/J for different L indicating a direct SN-VBS transition. The lower panel shows MC histories (and histograms in the inset) at $Q/J = 1.26$, providing clear evidence that the SN-VBS transition at $N = 7$ is direct and first-order.

description of our $\text{SO}(N)$ models is given by a RP^{N-1} theory (in contrast to the CP^{N-1} description of $\text{SU}(N)$ models [31]), which can be described as N real matter fields coupled to a Z_2 gauge field. Such a theory is expected to host three phases [32], a symmetry breaking phase in which the matter condenses (which we identify in our spin model as the SN), a stable phase in which the matter gets a gap and the Z_2 gauge theory is deconfined (identified here as the QSL) and a phase in which matter is gapped and the Z_2 is confined (identified here as the VBS). Thus, the SN-QSL critical point should be in the universality class of $\text{O}(N)^*$ critical point [3]. The QSL-VBS phase transition should be in the same universality class as the critical point between these identical phases in the quantum dimer model since the magnetic fluctuations are gapped in both the QSL and VBS phases. A previous analysis of this phase transition has predicted an $\text{O}(4)^*$ phase transition [27], where the VBS order parameter is identified with a bilinear of the primary field.

A detailed study of the critical phenomena at $N = 10$ and $N = 11$ is clearly beyond the scope of the current manuscript. We shall be satisfied here with a brief analysis: At the QSL-VBS critical point, we are able to carry out reasonable data collapses [15] at both $N = 10$ and $N = 11$ for O_{VBS}^2 (for both X and M ordering vectors, see Fig. 1) and R_{VBS} , where we find, $\eta_{\text{VBS}} = 1.3(2)$ and $\nu_{\text{VBS}} = 0.65(20)$ for the anomalous dimension of O_{VBS} . The unusually large value of η_{VBS} is a direct consequence

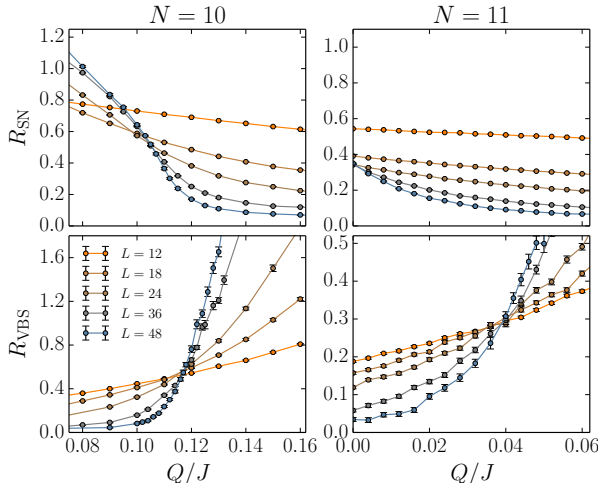


FIG. 5. Crossings of R_{SN} (above) and R_{VBS} (below) signaling the location of the onset of long-range SN and VBS orders at $N = 10$ (left) and $N = 11$ (right). At $N = 10$, R_{SN} and R_{VBS} cross at close but significantly different couplings, $Q_c = 0.100(5)$ and $Q_c = 0.117(2)$ respectively. At $N = 11$, R_{SN} appears to have crossed at $Q/J < 0$ (we cannot study this region because of the sign problem), whereas R_{VBS} crosses at $Q_c = 0.042(3)$. From the location of the crossings, for both $N = 10$ and $N = 11$, we can infer an intermediate phase which is neither SN nor VBS, as shown in Fig. 3(b). We present arguments that this phase is a QSL. No evidence for first order behavior is found at either of the transitions. The QSL-VBS transitions shows good scaling behavior with unconventional critical exponents.

of fractionalization in the intermediate QSL phase and is often regarded as a smoking gun diagnostic of exotic critical points (see e.g., [33]). More quantitatively, our critical exponents are in rough agreement with the best estimate of $\eta = 1.375(5)$ of the bilinear field and $\nu = 0.7525(10)$ in the $O(4)$ model [34]. We note that the values for η_{VBS} and ν_{VBS} agree within the quoted errors for $N = 10$ and $N = 11$. Taken together, this bolsters the case that the intermediate QSL phase has Z_2 fractionalization, albeit more work is needed for a definitive identification. Unfortunately, the SN-QSL transition, observed only at $N = 10$, has large corrections to scaling and we are unable to reliably determine its critical exponents.

In summary, we have introduced a new family of sign-free $SO(N)$ spin models, which can be regarded as non-bipartite generalizations of their popular $SU(N)$ cousins. The triangular lattice model which we have studied thoroughly here hosts a spin nematic, a VBS with a large unit cell, a quantum spin liquid phase and unusual quantum critical points. The absence in the $SO(N)$ models of a direct continuous “deconfined quantum critical point” [33] is in striking contrast to previous simulations of the related bipartite $SU(N)$ models [8, 23]. We have offered a plausible field theoretic scenario that naturally explains

this difference.

While the study in this paper has focussed on the triangular lattice, our family of models, Eq. (2,4) may be constructed sign free on any two or three dimensional non-bipartite lattice. Because of the larger degree of frustration, the kagome system may provide a wider swath of the QSL phase and hence could possibly allow a more detailed study of this phase, even if the phase diagram is of the same form found here. Exploring the phase diagram and quantum phase transitions of the three dimensional pyrochlore system is an open question for future work.

The author is grateful to J. Chalker, T. Lang, M. Levin, R. Mong, G. Murthy, A. Nahum, A. Sandvik, T. Senthil and M. Zaletel for helpful discussions. This research was supported in part by NSF DMR-1056536.

- [1] L. Balents, *Nature* **464**, 199 (2010), URL <http://dx.doi.org/10.1038/nature08917>.
- [2] S. Sachdev, *Quantum Phase Transitions* (Cambridge University Press, 1999).
- [3] C. Xu, *Int. J. Mod. Phys. B* p. 1230007 (2012).
- [4] C. Wu, *Physics* **3**, 92 (2010).
- [5] B. Sutherland, *Phys. Rev. B* **12**, 3795 (1975), URL <http://link.aps.org/doi/10.1103/PhysRevB.12.3795>.
- [6] I. Affleck, *Phys. Rev. Lett.* **54**, 966 (1985), URL <http://link.aps.org/doi/10.1103/PhysRevLett.54.966>.
- [7] N. Read and S. Sachdev, *Phys. Rev. Lett.* **62**, 1694 (1989), URL <http://link.aps.org/doi/10.1103/PhysRevLett.62.1694>.
- [8] R. K. Kaul, R. G. Melko, and A. W. Sandvik, *Annu. Rev. Cond. Matt. Phys.* **4**, 179 (2013), URL <http://www.annualreviews.org/doi/abs/10.1146/annurev-conmatphys-030212-184215>.
- [9] N. Read and S. Sachdev, *Phys. Rev. Lett.* **66**, 1773 (1991), URL <http://link.aps.org/doi/10.1103/PhysRevLett.66.1773>.
- [10] E. Demler, W. Hanke, and S.-C. Zhang, *Rev. Mod. Phys.* **76**, 909 (2004), URL <http://link.aps.org/doi/10.1103/RevModPhys.76.909>.
- [11] H.-H. Tu, G.-M. Zhang, and T. Xiang, *Phys. Rev. B* **78**, 094404 (2008), URL <http://link.aps.org/doi/10.1103/PhysRevB.78.094404>.
- [12] F. Alet, S. Capponi, H. Nonne, P. Lecheminant, and I. P. McCulloch, *Phys. Rev. B* **83**, 060407 (2011), URL <http://link.aps.org/doi/10.1103/PhysRevB.83.060407>.
- [13] K. Okunishi and K. Harada, *Phys. Rev. B* **89**, 134422 (2014), URL <http://link.aps.org/doi/10.1103/PhysRevB.89.134422>.
- [14] Strictly speaking the symmetry of our model is an $SO(N)$ for odd- N and an $O(N)/Z_2$ for even N . This point is discussed further in the supplementary materials.
- [15] Please refer to supplementary materials for more details on the model and the numerical simulations.
- [16] G. Santoro, S. Sorella, L. Guidoni, A. Parola, and E. Tosatti, *Phys. Rev. Lett.* **83**, 3065 (1999), URL <http://link.aps.org/doi/10.1103/PhysRevLett.83.3065>.
- [17] K. Harada, N. Kawashima, and M. Troyer, *Phys. Rev. Lett.* **90**, 117203 (2003), URL <http://journals.aps.org/doi/10.1103/PhysRevLett.90.117203>.

[org/prl/abstract/10.1103/PhysRevLett.90.117203](http://prl.org/prl/abstract/10.1103/PhysRevLett.90.117203).

[18] K. S. D. Beach, F. Alet, M. Mambrini, and S. Capponi, Phys. Rev. B **80**, 184401 (2009), URL <http://link.aps.org/doi/10.1103/PhysRevB.80.184401>.

[19] J. Lou, A. Sandvik, and N. Kawashima, Phys. Rev. B **80**, 180414 (2009), URL <http://link.aps.org/doi/10.1103/PhysRevB.80.180414>.

[20] R. K. Kaul, Phys. Rev. B **85**, 180411 (2012), URL <http://link.aps.org/doi/10.1103/PhysRevB.85.180411>.

[21] R. K. Kaul and A. W. Sandvik, Phys. Rev. Lett. **108**, 137201 (2012), URL <http://link.aps.org/doi/10.1103/PhysRevLett.108.137201>.

[22] M. S. Block and R. K. Kaul, Phys. Rev. B **86**, 134408 (2012), URL <http://link.aps.org/doi/10.1103/PhysRevB.86.134408>.

[23] M. S. Block, R. G. Melko, and R. K. Kaul, Phys. Rev. Lett. **111**, 137202 (2013), URL <http://link.aps.org/doi/10.1103/PhysRevLett.111.137202>.

[24] R. K. Kaul, Phys. Rev. B **86**, 104411 (2012), URL <http://link.aps.org/doi/10.1103/PhysRevB.86.104411>.

[25] A. Laeuchli, F. Mila, and K. Penc, Phys. Rev. Lett. **97** (2006).

[26] N. Read and S. Sachdev, Nuclear Physics B **316**, 609 (1989), ISSN 0550-3213, URL <http://www.sciencedirect.com/science/article/pii/0550321389900618>.

[27] R. Moessner and S. L. Sondhi, Phys. Rev. B **63**, 224401 (2001), URL <http://link.aps.org/doi/10.1103/PhysRevB.63.224401>.

[28] A. Ralko, M. Ferrero, F. Becca, D. Ivanov, and F. Mila, Phys. Rev. B **74**, 134301 (2006), URL <http://link.aps.org/doi/10.1103/PhysRevB.74.134301>.

[29] A. W. Sandvik, AIP Conf. Proc. **1297**, 135 (2010), URL <http://scitation.aip.org/content/aip/proceeding/aipcp/10.1063/1.3518900>.

[30] A. W. Sandvik, Phys. Rev. Lett. **98**, 227202 (2007), URL <http://link.aps.org/doi/10.1103/PhysRevLett.98.227202>.

[31] N. Read and S. Sachdev, Phys. Rev. B **42**, 4568 (1990).

[32] P. E. Lammert, D. S. Rokhsar, and J. Toner, Phys. Rev. Lett. **70**, 1650 (1993), URL <http://link.aps.org/doi/10.1103/PhysRevLett.70.1650>.

[33] T. Senthil, A. Vishwanath, L. Balents, S. Sachdev, and M. P. A. Fisher, Science **303**, 1490 (2004), URL <http://www.sciencemag.org/content/303/5663/1490.abstract>.

[34] H. Ballesteros, L. Fernndez, V. Martn-Mayor, and A. M. Sudupe, Physics Letters B **387**, 125 (1996), ISSN 0370-2693, URL <http://www.sciencedirect.com/science/article/pii/0370269396009847>.

[35] R. G. Melko, A. Paramekanti, A. A. Burkov, A. Vishwanath, D. N. Sheng, and L. Balents, Phys. Rev. Lett. **95**, 127207 (2005), URL <http://link.aps.org/doi/10.1103/PhysRevLett.95.127207>.

[36] D. Heidarian and K. Damle, Phys. Rev. Lett. **95**, 127206 (2005), URL <http://link.aps.org/doi/10.1103/PhysRevLett.95.127206>.

[37] S. Wessel and M. Troyer, Phys. Rev. Lett. **95**, 127205 (2005), URL <http://link.aps.org/doi/10.1103/PhysRevLett.95.127205>.

[38] M. B. Hastings, Phys. Rev. B **69**, 104431 (2004).

[39] K. Harada, Phys. Rev. E **84**, 056704 (2011), URL <http://link.aps.org/doi/10.1103/PhysRevE.84.056704>.

SUPPLEMENTARY MATERIALS

Model and Symmetries

Here we provide some additional details of the models introduced in Eq. (1) and Eq. (2).

Mapping between Eqs. (1) and (2)

To see the connection between the two Hamiltonians Eq. (1) and Eq. (2). We consider two $SO(N)$ spins. We can combine them into three representations: a singlet (S), symmetric (χ) and anti-symmetric (Φ) representations of dimensions: 1 , $\frac{N^2}{2} + \frac{N}{2} - 1$ and $\frac{N^2}{2} - \frac{N}{2}$. Now construct projectors on these representations, P_S , P_χ and P_Φ . Clearly $P_S + P_\chi + P_\Phi = 1$ and $P_S^2 = P_S$, $P_\chi^2 = P_\chi$, $P_\Phi^2 = P_\Phi$. It is straightforward to show that, $(L_i \cdot L_j) = -(N-1)P_S - P_\chi + P_\Phi$ by explicitly acting on the symmetrized wave-functions. From this it follows that $(L_i \cdot L_j)^2 = (N-1)^2 P_S + P_\chi + P_\Phi$. From which it follows that $(L_i \cdot L_j)^2 = ((N-1)^2 - 1) P_S + 1$, which proves as claimed that for $N \geq 3$, Eq. (1) and Eq. (2) are equivalent up to a constant.

$$N = 2$$

Although not studied in this manuscript, for the sake of completeness, we discuss our model at $N = 2$. Even though Eq. (1) is trivial for $N = 2$ (since squaring the only $SO(2)$ generator is just an identity operator), Eq. (2) is a well defined non-trivial model. Identifying the two colors with \uparrow and \downarrow spins, Eq. (2) becomes $\hat{H} = \sum_{\langle ij \rangle} -J(S_i^x S_j^x + S_i^z S_j^z) + JS_i^y S_j^y$. Previous work on the triangular lattice $N = 2$ model has found clear evidence for $SO(2)$ symmetry breaking superfluid order [35–37].

Symmetries

We now discuss the symmetries of the model Eq. (2). We begin by observing that this model is invariant under uniform $O(N)$ rotations where we multiply each basis state by an orthogonal matrix (one that satisfies $O^T O = 1$), since this leaves the singlet state invariant, *i.e.*

$$\sum_{\alpha} |\alpha\alpha\rangle \rightarrow \sum_{\alpha} O_{\alpha\gamma} O_{\alpha\eta} |\gamma\eta\rangle = \sum_{\alpha} |\alpha\alpha\rangle. \quad (5)$$

However we should identify rotations that only differ by changing all the local basis states by the same phase (in this case a sign). Here it becomes necessary to distinguish between even and odd N . This is because the matrix -1 has determinant 1 for even N and -1 for odd N . Thus

for odd- N the symmetry is simply $SO(N)$, since the rest of $O(N)$ is obtained from $SO(N)$ by multiplying by -1. For even- N however $SO(N)$ has pairs of elements that cause the same basis transformation up to a sign, *e.g.* 1 and -1. On the other hand unlike the case of odd- N , the $O(N)$ matrices with determinant -1 are independant symmetries, so the symmetry realized for even- N is an $\frac{O(N)}{Z_2}$.

Symmetry on Bipartite Lattices

On bipartite lattices the orthogonal rotation symmetry, Eq. (5) gets extended to a unitary symmetry (with $U^\dagger U = 1$) so long as the singlet is defined between sites on opposite sub-lattices, and A sub-lattice spins are rotated by U and B sub-lattice spins are rotated by U^* ,

$$\sum_{\alpha} |\alpha\alpha\rangle \rightarrow \sum_{\alpha} U_{\alpha\gamma}^* U_{\alpha\eta} |\gamma\eta\rangle = \sum_{\alpha} |\alpha\alpha\rangle. \quad (6)$$

Since a uniform phase change of the all the states locally does not have physical consequences, the model is said to have an $SU(N)$ symmetry, as has been discussed and extensively studied previously in such models, see *e.g.* Ref. [8] for a review.

Ground state theorems

Marshall's sign theorem guarantees that the ground state of $H_{JQ} = H_J + H_Q$ is an $SO(N)$ singlet. In addition, on the triangular lattice, which is the focus of our study here, there is no simple translationally invariant covering of two-site singlets, leading us to suspect that a generalization of the $SU(2)$ square lattice Lieb-Schultz Mattis (LSM) theorem [38] applies to H_{JQ} on this lattice, *i.e.* in the thermodynamic limit there must be a degeneracy in the ground state, so that a simple gapped paramagnet is not possible – either a symmetry is broken or the ground state is exotic. A rigorous proof of this intuitive assertion is expected to be at least as technical as the proof for the bipartite $N = 2$ case [38] and is beyond the scope of this work. As we saw above, on a one-dimensional chain, which is bipartite, our model is equivalent to the $SU(N)$ model studied by Affleck [6] and is hence expected to have an LSM degeneracy.

Numerical Simulations

QMC energy tests

Here we provide the results of some QMC tests on small lattices for the total energy per spin of our models, $\hat{H}_J + H_Q$, Eqs. (2,4) on the triangular lattice, for completeness and future comparisons.

size	N	Q	β_{QMC}	E_{ex}	E_{QMC}
2×2	4	0	16	-1.5	-1.49997(3)
2×2	4	1	16	-4.5	-4.5000(1)
2×2	5	0	16	-1.4	-1.40000(5)
2×2	5	1	16	-4.2	-4.2001(1)
2×3	3	2	16	-6.0657499233	-6.0656(1)
3×3	2	0	16	-1.7026987262	-1.70269(2)
3×3	2	1	16	-3.7290340614	-3.72900(3)
3×3	2	2	16	-5.7639923092	-5.76402(5)

TABLE I. Test comparisons of ground state energies from exact diagonalization and average energies from finite- T QMC studies of the $\text{SO}(N)$ model introduced here. Note that $J = 1$ always. The energies reported here are per site and on triangular lattices with periodic boundary conditions such that there are always $3L^2$ bonds and $3L^2$ plaquettes in Eqs. (2,4). This causes some terms to appear more than once for the 2×2 and 2×3 systems.

Choice of $\beta = L$

In Fig. 6 we show the dependence of the fluctuations of the temporal and spatial winding numbers on the “aspect ratio” of our simulation cell. β is a measure of the extent of the imaginary time and L is an estimate for the linear spatial extent. We study the fluctuations of the temporal and spatial winding numbers as the ratio β/L is varied for two different sizes, $L = 32$ and $L = 48$ at $N = 10$ in the model \hat{H}_J . We find that both quantities are balanced at a value of β/L which is of the order of one (close to 1.42) and that the crossing point does not move much with system size. Thus for simplicity we have chosen $\beta/L = 1$ throughout the paper.

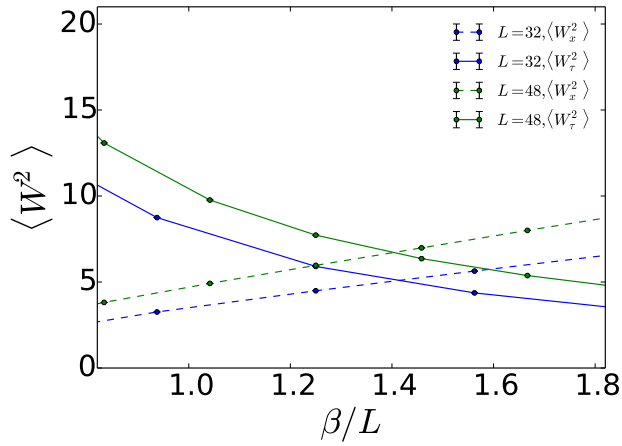


FIG. 6. Estimation of optimal β/L ratio for our simulations by comparison of the fluctuations of the temporal ($\langle W_\tau^2 \rangle$) and spatial ($\langle W_x^2 \rangle$) winding numbers. Data shown is for \hat{H}_J at $N = 10$.

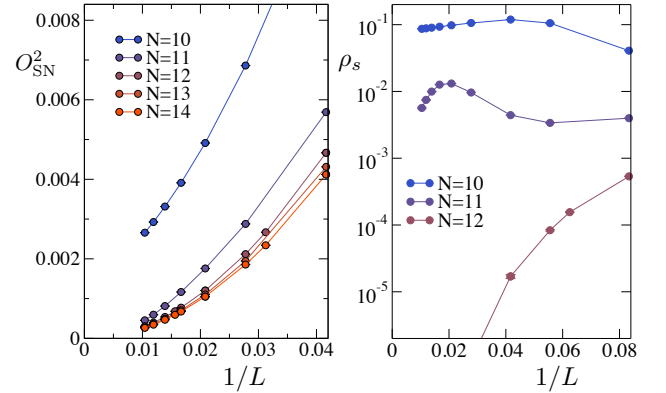


FIG. 7. Finite size scaling of spin nematic order parameter and spin stiffness for the model \hat{H}_J , in Eq. (1) with $10 \leq N \leq 14$. Shown on the left is the square of the spin nematic order parameter, O_{SN}^2 (the height of the Bragg peak in Fig. 1), and on the right is the spin stiffness, ρ_s , plotted as a function of $1/L$. The data confirms that the system is magnetically ordered for $N \leq 10$ and non-magnetic for $N \geq 11$.

Extrapolation of order parameter

To test quantitatively for long range order we study the scaling of the height of the peak in $S_M(\mathbf{k})$, $O_M^2 \equiv S_M(\mathbf{k} = 0)$ and the spin stiffness ρ_s on finite size systems with $N_{\text{site}} = L \times L$. Both quantities are expected to be finite in the M state and zero when the $O(N)$ symmetry is restored. Fig. 7 shows finite size data for both quantities for different values of N . From these plots we conclude that the M symmetry is broken up to $N = 10$ and is restored for $N \geq 11$, because O_M^2 scales to zero for these N . This behavior is mirrored in ρ_s , albeit for intermediate L there is some non-monotonic behavior for $N = 11$. This is consistent with our conclusions in the main text made from the analysis of R_{SN}

QSL-VBS critical point

We obtain critical exponents at the QSL-VBS critical point by attempting a data collapse, see Fig. 8,9. We use the standard finite size scaling ansatz for the order parameter and the crossing ratio,

$$\langle O_{\text{VBS}}^2 \rangle = L^{-(1+\eta_{\text{VBS}})} \mathcal{F}_O(gL^{1/\nu_{\text{VBS}}}) \quad (7)$$

$$R_{\text{VBS}} = \mathcal{F}_R(gL^{1/\nu_{\text{VBS}}}) \quad (8)$$

where $g = (Q - Q_c)/J$. We continue to work with $\beta = L$ as discussed. No attempt is made to make use of corrections to this leading scaling behavior. Our main objective is to determine the universal number η_{VBS} for the QSL-VBS transition for $N = 10$ and $N = 11$. We find

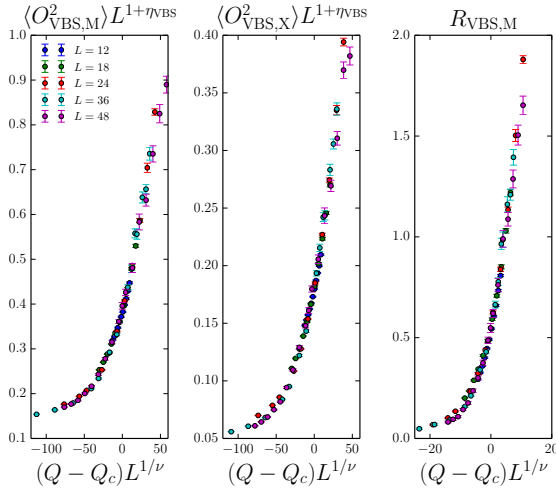


FIG. 8. Examples of our data collapses at QSL-VBS critical point at $N = 10$ shown here with the best parameters determined individually for each observable. The parameters used are $Q_c = 0.1170, 0.1187, 0.1171$, $1/\nu_{VBS} = 2.171, 2.152, 1.733$ and $\eta_{VBS} = 1.414, 1.106, -$.

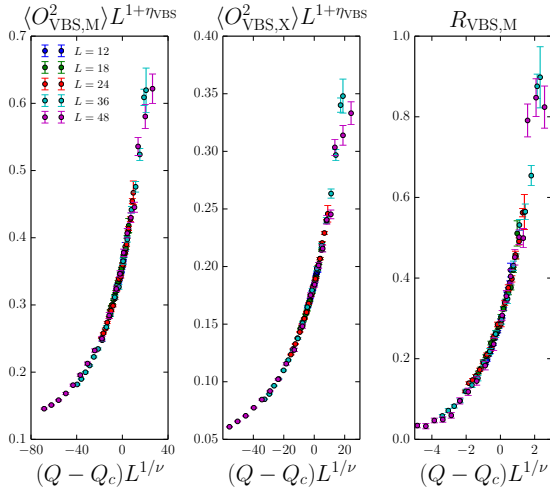


FIG. 9. Examples of our data collapses at QSL-VBS critical point at $N = 11$ shown here with the best parameters determined individually for each observable. The parameters used are $Q_c = 0.04330, 0.04182, 0.03917$, $1/\nu_{VBS} = 1.902, 1.858, 1.244$ and $\eta_{VBS} = 1.383, 1.133, -$.

acceptable collapses for our data sets over a wide range of ν_{VBS} . On the other hand, the estimate for η_{VBS} is relatively stable over our various fits. The values and errors of the critical exponents quoted in the main text are based on the variation observed by using different data sets. A higher precision study should be possible with access to more accurate data and larger system sizes. In order to carry out the collapse numerically, we make use of a recently developed Bayesian approach to scaling [39].